Available online at www.sciencedirect.com
SCIENCE DIRECT
Journal of Catalysis 242 (2006) 71–81
JOURNAL OF CATALYSIS
www.elsevier.com/locate/jcat

Role of gold cations in the oxidation of carbon monoxide catalyzed by iron oxide-supported gold

Graham J. Hutchings [a,*], Matthew S. Hall [a], Albert F. Carley [a], Philip Landon [a], Benjamin E. Solsona [a], Christopher J. Kiely [b], Andrew Herzing [b], Michiel Makkee [c], Jacob A. Moulijn [c], Arian Overweg [d], Juan Carlos Fierro-Gonzalez [e], Javier Guzman [e], Bruce C. Gates [e]

[a] *School of Chemistry, Cardiff University, Main Building, Park Place, Cardiff, CF10 3AT, UK*
[b] *Center for Advanced Materials and Nanotechnology, Lehigh University, 5 East Packer Avenue, Bethlehem, PA 18015, USA*
[c] *DelftChemTech, Reactor & Catalysis Engineering, Faculty of Applied Sciences, Delft University of Technology, Julianalaan 136, 2628 BL Delft, The Netherlands*
[d] *Department of Radiation, Radionuclides & Reactors, Faculty of Applied Sciences, Delft University of Technology, Mekelweg 15, 2629 JB Delft, The Netherlands*
[e] *Department of Chemical Engineering and Materials Science, University of California, Davis, CA 95616, USA*

Received 7 February 2006; revised 1 June 2006; accepted 2 June 2006

Available online 30 June 2006

Abstract

Recent intense interest in catalysis by supported gold has focused mainly on the oxidation of CO at low temperatures, which offers the potential for many important applications, including the purification of hydrogen for automotive fuel cells. Numerous, contradictory proposals have been made concerning the nature of the active sites in supported gold catalysts. We now present evidence from a set of complementary experimental methods characterizing Au/α-Fe_2O_3 catalysts, demonstrating that cationic gold plays a crucial role in catalyzing CO oxidation at 298 K, as well as in the hydrogenation of crotonaldehyde. A series of catalysts based on a co-precipitated 5-wt% Au/Fe_2O_3 precursor heat treated in different ways were compared for CO oxidation at ambient temperature. The catalysts were structurally and chemically analyzed by HREM and STEM-XEDS. A combination of EXAFS, in situ XANES, XPS, and Mössbauer effect spectroscopy demonstrates the important role of cationic gold in the activity of these iron oxide-supported gold catalysts.

Keywords: Gold; Oxidation state; Catalysis; XANES; STEM-XEDS, Mössbauer spectroscopy, XPS; CO oxidation

1. Introduction

Gold highly dispersed on metal oxide supports has unexpectedly been found to be highly active for a number of catalytic reactions, including vinyl chloride synthesis from the hydrochlorination of acetylene, [1–4] propene epoxidation using hydrogen as a sacrificial reductant, [5–8] hydrogenation of unsaturated aldehydes, [9,10] and CO oxidation [11–20]. Recently, gold-containing catalysts have been found to be highly efficient for the direct oxidation of hydrogen to produce hydrogen peroxide [21–27], as well as the oxidation of alcohols [28–33]. Most recently, alkene epoxidation in the absence of sacrificial hydrogen has been achieved [34]. However, although there is considerable interest in investigating new gold catalysts and gold-catalyzed reactions, most research interest has been focused on understanding the role of gold in the activation and oxidation of CO. These studies have involved two types of experimental investigation, namely those concerned with finely dispersed gold nanoparticles [15] on high-area supports and those based on theoretical and model investigations using single-crystal oxide surfaces with highly controlled gold structures [16]. Comparing data acquired using these two approaches clearly demonstrates that the electronic nature of the gold species in active catalysts has not been fully elucidated, and highly active catalysts can be prepared using TiO_2 [18], CeO_2 [19], and Fe_2O_3 [20] as supports.

* Corresponding author. Fax: +44 (0) 29 2087 4030.
E-mail address: hutch@cardiff.ac.uk (G.J. Hutchings).

0021-9517/$ – see front matter
doi:10.1016/j.jcat.2006.06.001

A key issue that remains unresolved concerns the role of cationic gold in the oxidation of CO in these high-activity catalysts. Some studies have suggested a role for gold cations [19,20,37,38]; however, it is unclear whether cationic gold alone or in combination with metallic gold in these catalysts acts as the active species, or whether small residues of metallic gold compose the active centers. A number of model studies [39–41] led mainly to the conclusion that just the metallic form of gold is active. The species that catalyze CO oxidation in model catalysts dispersed on planar hydroxyl-free surfaces have been variously identified as gold nanoclusters [39] or layers [40] on single-crystal metal oxide supports with size-dependent electronic and chemical properties [41,42], gold anions occupying defect sites on supports [43], and low-coordinated gold atoms in nanoclusters [44]. However, the structures of the model catalysts differ significantly from those of catalysts used in large-scale commercial applications. Furthermore, in no investigation with model catalysts was there any reported attempt to test for the presence of cationic gold. On the other hand, gold cations alone on a zeolite [35] and on La_2O_3 [36] have been identified as catalytic sites for CO oxidation catalysis, and gold cations in the presence of zerovalent gold nanoclusters on partially hydroxylated MgO have been found to increase the catalytic activity [37]. Cationic gold has also been deemed important in lanthanide-supported gold catalysts [19,37,38,45].

The current debate on the oxidation state of gold in active supported gold catalysts arises in part from the fact that interpreting the results of individual spectroscopic techniques that provide information about the oxidation state of supported metals is not straightforward. Here we attempt to provide some insight into the interpretation of CO oxidation catalysis by supported gold, reporting evidence of the structure and oxidation states of gold in Fe_2O_3-supported catalysts determined by a set of independent yet complementary physical methods, including characterization of the catalysts in the functioning state. The data clearly demonstrate the involvement of gold cations in the catalysis of CO oxidation with our "real" high-activity nanocrystalline catalyst dispersed on a hydroxylated iron oxide support. Moreover, this highly detailed study considerably extends our previous investigations of CO oxidation on Au/Fe_2O_3 [20,46].

2. Experimental

2.1. Preparation of iron oxide-supported catalysts

Au/Fe_2O_3 catalysts were prepared by co-precipitation. Dilute aqueous solutions of $HAuCl_4{\cdot}3H_2O$ and $Fe(NO_3)_3{\cdot}9H_2O$ containing the calculated amounts of Au and Fe required to give the desired loading on Fe_2O_3 were mixed together under stirring at 353 K. Na_2CO_3 (0.25 mol l^{-1}) was added dropwise until a pH 8.2 was attained. The resulting precipitate was then recovered by filtration and washed with hot deionized water (353 K, 1 l). The material was then treated in three different ways: (i) A sample was dried at 393 K in flowing air; (ii) a sample was dried at 393 K in static air; and (iii) a sample was calcined at 673 K in flowing air. Table 1 summarizes the samples prepared and studied in this investigation.

Table 1
Summary of samples and various heat treatment (HT) conditions

Sample ID*	Heat treatment	HT atmosphere	HT time
A	Dried, 393 K	Flowing air	8 h
B	Calcined, 693 K	Flowing air	3 h
C	Dried, 393 K	Flowing air	8 h
D	Dried, 393 K	Static air	8 h
E	Dried, 393 K	Flowing air	8 h
F	Calcined, 693 K	Flowing air	4 h

* All samples contained 5-wt% gold.

2.2. Catalyst testing: CO oxidation

Catalyst samples (50 mg) were evaluated for CO oxidation using a fixed-bed reactor (i.d. = 3 mm). The standard test conditions were as follows: CO (flow rate, 0.5 ml min^{-1}), He (4.5 ml min^{-1}), and O_2 (50 ml min^{-1}), with total gas space velocity of 66,000 ml of gas (g of catalyst)$^{-1}$ h^{-1} fed to the reactor (held at 293 K) using mass flow controllers. The product gases were analyzed by on-line gas chromatography, and the conversion of CO and formation of CO_2 were both quantified. Catalysts were evaluated for crotyl alcohol formation by hydrogenation of crotonaldehyde, as described previously [10]. After being used in the reactor, the catalysts were stored at room temperature in sealed containers before spectroscopic analysis (Section 2.3). Under such conditions, the state of the catalyst surface will be unaffected; in particular, the oxidation state of the gold particles will remain unchanged.

2.3. Catalyst characterization

2.3.1. X-ray photoelectron spectroscopy

XPS spectra were recorded with three spectrometers: a Scienta ESCA 300 instrument at the National Centre for Electron Spectroscopy and Surface Analysis, Daresbury, Cheshire, UK, and a custom-made spectrometer (VG Scientific) and a VG ESCALAB 220 spectrometer, both at Cardiff. A monochromatic AlK_α source was used with the Scienta instrument, and a standard AlK_α source was used with the ESCALAB instrument.

2.3.2. X-ray absorption spectroscopy

EXAFS and XANES spectra characterizing the iron oxide-supported Au catalysts were recorded at X-ray beamline X-18B at the National Synchrotron Light Source, Brookhaven National Laboratory. The storage ring energy was 2.8 GeV, and the ring current varied within the range of 110–250 mA. XAS spectra were recorded at the Au L_{III} edge (11,919 eV) in fluorescence mode. In some experiments, the samples were loaded into a XAS cell [47] aligned in the X-ray beam, and the data were recorded at room temperature and atmospheric pressure. In other experiments, the samples were loaded into an in situ XAS cell [48], and data were collected during CO oxidation catalysis. The Si(111) double-crystal monochromator was detuned by 20% at the Au L_{III} edge to suppress higher harmonics

in the X-ray beam. EXAFS data were analyzed by a difference-file technique embedded in the XDAP program [49], and the features in the XANES spectra were compared with those of reference materials containing gold in known oxidation states. Iterative fitting was carried out until excellent agreement was attained between the calculated k^0-, k^1-, and k^2-weighted data (where k is the photoelectron wave vector) and the postulated model. The number of parameters used in fitting the data to each model was justified statistically by the Nyquist theorem.

2.3.3. Mössbauer effect spectroscopy

The experiments were performed with Mössbauer sources created by irradiating platinum powder, enriched in ^{196}Pt (97%) with thermal neutrons. The resultant ^{197}Pt decays to the Mössbauer isotope ^{197}Au. The 77.3-keV gamma Mössbauer line was used; because of this line's high energy, the recoil-free fraction (i.e., the fraction of gamma emissions and absorptions that occur recoil-free, which can be used for the Mössbauer effect) was negligible at temperatures above 30 K. Therefore, both the source and the absorber were cooled to 4.2 K in a special helium bath-type cryostat. The spectrum was calibrated by recording a spectrum of sodium nitroprusside using a ^{57}Co:Rh source; absolute velocities are reported.

2.3.4. Electron microscopy measurements

Samples of each catalyst were prepared for examination by TEM by dispersing the catalyst powder in high-purity ethanol. A drop of the suspension was then allowed to evaporate on a holey-carbon film supported by a 300-mesh copper TEM grid. Bright field imaging experiments were carried out on a JEOL 2000FX TEM instrument operating at 200 kV with a LaB_6 source. High-resolution lattice imaging was performed in a JEOL 2010 FEG-TEM operating at 200 kV. In addition, high-angle annular dark-field (HAADF) imaging was carried out on a VG HB603 dedicated scanning transmission electron microscope operating at 300 kV, which was also equipped with an Oxford Instruments Inca software package for X-ray energy dispersive spectroscopic (XEDS) mapping.

3. Results and discussion

This investigation focused on gold supported on α-Fe_2O_3 prepared by co-precipitation, which has been found to be one of the most active and stable catalysts yet reported for CO oxidation [20,46]. We have previously shown [20] that the heat treatment to which the precipitate is subjected can control the catalytic activity for CO oxidation—in particular, as the calcination temperature is increased, the activity decreases. Here we have extended this earlier work, which was based on only a few catalyst samples, and have analyzed a larger selection of iron oxide-supported gold catalysts prepared using co-precipitation and subjected to various subsequent heat treatments. We again confirmed that the thermal history of the samples indeed has a profound influence on the activities of the catalysts for this reaction. In particular, we found that high activity was generally associated with samples dried at 393 K, whereas low activity was associated with catalysts heat-treated at 673 K.

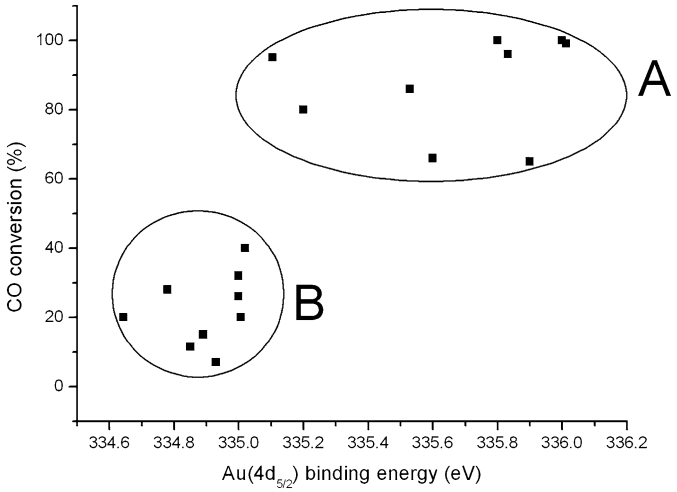

Fig. 1. Correlation between activity for CO conversion and Au($4d_{5/2}$) binding energy. The data for a series of catalysts (5-wt% Au supported on Fe_2O_3) are shown; the cluster of points labeled A corresponds to catalysts dried at 393 K, and the cluster B to those calcined at 673 K.

XPS data characterizing catalysts prepared using these two heat treatment regimes showed a broad correlation between CO conversion and Au($4d_{5/2}$) core-level binding energy (Fig. 1). These data clearly clustered into two groups. One group of catalyst samples dried at 393 K (labeled A) corresponded to high conversion (65–100%) and was generally associated with a higher Au($4d_{5/2}$) binding energy than the less active group (B), calcined at 673 K.

We found that these 5-wt% Au/Fe_2O_3 materials also catalyzed the hydrogenation of crotonaldehyde. Catalysts in group A were effective for crotonaldehyde hydrogenation, whereas those in group B were typically much less active and often showed no activity when tested under our standard conditions. High-resolution Au(4f) spectra obtained on the Scienta spectrometer, representing an active (60% conversion) and a poorly active catalyst (20% conversion) for crotonaldehyde hydrogenation (Fig. 2), showed that the former contained a mixture of cationic and metallic gold, whereas the latter had metallic gold without detectable cationic gold. The curve-fit analysis shown in Fig. 2a indicates two components to the Au(4f) spectrum, separated by 0.8 eV, with contributions of cationic gold and metallic gold to the signal intensity of 41 and 59%, respectively.

Because low conversion of CO or crotonaldehyde is associated with catalysts calcined at high temperature, these XPS data suggest that one or both of the following mechanisms is occurring:

(a) Calcination of the catalyst at higher temperatures leads to sintering of the gold nanoparticles, with the increase in cluster size reflected by a decreased Au($4d_{5/2}$) binding energy toward the value characteristic of the bulk metal [50]. (It is well established [15,16] that CO oxidation at room temperature is inefficient for particle sizes > ca. 8–10 nm.)
(b) The most active catalysts contain more cationic gold, and the least active catalysts contain more Au^0, with the bind-

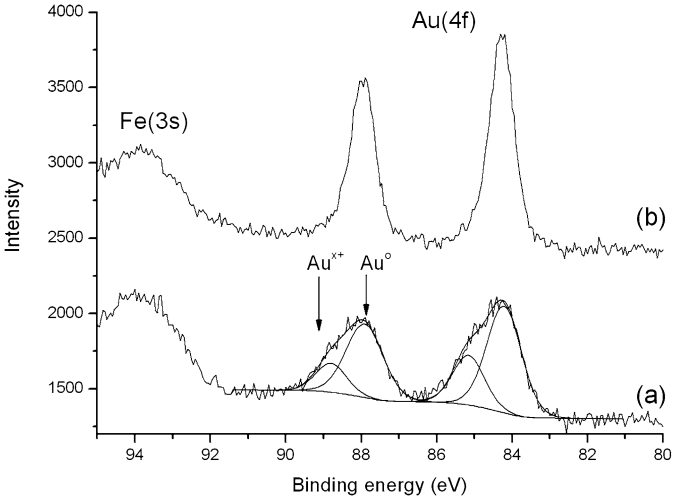

Fig. 2. High-resolution Au(4f) spectra obtained for a 5-wt% Au/Fe_2O_3 catalyst: (a) with a relatively high conversion (60%) for the hydrogenation of crotonaldehyde to crotyl alcohol, and (b) after calcination at 673 K, which reduced the conversion to 20%.

ing energy difference observed arising from the difference in charges on the gold species.

But this issue cannot be resolved using just a single technique, such as XPS. This limitation is particularly true for XPS, because final state effects associated with particle size can dominate the spectra [51–54]. We note that in principal, the initial state effects, reflecting the gold's electronic nature, can be checked by measuring the Auger parameter, but that this measurement is difficult for gold because of the high kinetic energies (2016 and 2102 eV) of the relevant Auger feature. We attempted to measure this Auger parameter for the catalysts in this study, but this proved impossible for our sample array because of the low Au concentration and consequent poor signal intensity. In an attempt to resolve this dilemma, we carefully chose a subset of samples and analyzed each using a set of complementary techniques; in all cases, only fresh samples were evaluated.

Initially, we chose two representative samples of 5-wt% Au/α-Fe_2O_3, one dried at 393 K in flowing air for 8 h (denoted as type A) and the other calcined in flowing air at 673 K (type B), corresponding to the high-activity and low-activity regions identified in Fig. 1. We evaluated these samples using a wide range of techniques to determine the nature of the active gold species. We characterized the gold in the catalysts with extended X-ray absorption fine structure spectroscopy (EXAFS), high-resolution transmission electron microscopy (HRTEM), and scanning transmission electron microscopy (STEM) with XEDS mapping to determine gold cluster sizes. We applied these techniques in concert with X-ray absorption near-edge structure (XANES) and XPS, which provide information about the gold oxidation states.

The STEM (Fig. 3) and EXAFS (Fig. 4; Table 2) data provide clear evidence of particles of gold in the catalysts. The EXAFS data (Fig. 4; Table 2) provide only average structural information about these gold nanoparticles, showing a difference in average particle size indicated by the Au–Au first-shell CNs of 8.3 for the dried sample and 10.7 for the calcined sample. To determine the sizes of individual gold nanoparticles, we carried out detailed STEM and HREM analyses of the two samples. Distinct gold nanoparticles were evident in the images of both samples A and B. The mean diameter of gold nanoparticles in sample A was 3.8 nm, and that of the nanoparticles in sample B was 8.2 nm (Fig. 3). In view of the uncertainties in these data, these results are consistent with the EXAFS results characterizing these samples (Table 2). The metal–metal (interatomic) distance is expected to decrease for smaller particle sizes in response to the vapor pressure above the more highly curved surface.

At first glance, these data appear to be consistent with models showing that the activity of supported gold catalysts is associated with gold nanoparticles in the 2–5 nm range [15], such as those observed in sample A but not in sample B. However, the XPS spectra representing samples that are typical of groups A and B show distinctly different signals for gold (Fig. 2). The XPS data representing group A samples can be explained in two ways: (1) There is a contribution of cationic gold, and (2) there is a distinct bimodal size distribution of gold nanocrystals.

The latter interpretation is not consistent with the STEM analysis reported here for samples A and B, because we did not observe a bimodal gold particle size distribution. It could be argued at this point that even if cationic gold were present, as indicated by the combined XPS and STEM data, this could be a spectator species not relevant to the catalysis, as suggested recently by Chen and Goodman [55], and the differences in activity could arise solely from the different sizes of metallic gold particles.

To pursue this issue, and to obtain more information on gold oxidation states, we analyzed samples A and B by XANES (Fig. 5). The XANES spectrum of the most active catalyst (sample A) showed features indicating predominantly cationic gold, with some small contribution from Au^0, whereas features representing Au^0 dominated in the spectrum of the catalyst exhibiting low activity (sample B). Most importantly, the in situ XANES analysis (Fig. 5), measured as catalytic CO oxidation was occurring, showed that the samples were stable in flowing CO and air under reaction conditions at ambient temperature. Taken together, the XPS and XANES data suggest an important role for cationic gold in the CO oxidation catalysis, and we have investigated this possibility further.

Clearly, the thermal treatment of the initial precipitate controls the activity of these catalysts; indeed, iron oxide-supported gold catalysts may be unique in this respect. This sensitivity to thermal history is highlighted by measurements of two samples (denoted as C and D; Table 1) prepared by drying the precipitate at 393 K under different conditions. Sample C was treated in a tube furnace; sample D, in a GC oven.

Both of these samples were subjected to detailed STEM analysis (Fig. 6) and found to be very similar to each other with respect to gold particle size distributions (sample C, mean particle diameters, 7.0 nm for sample C and 5.4 nm for sample D). If the key catalyst property were the gold nanoparticle size, as has been proposed elsewhere [12,15], then these two

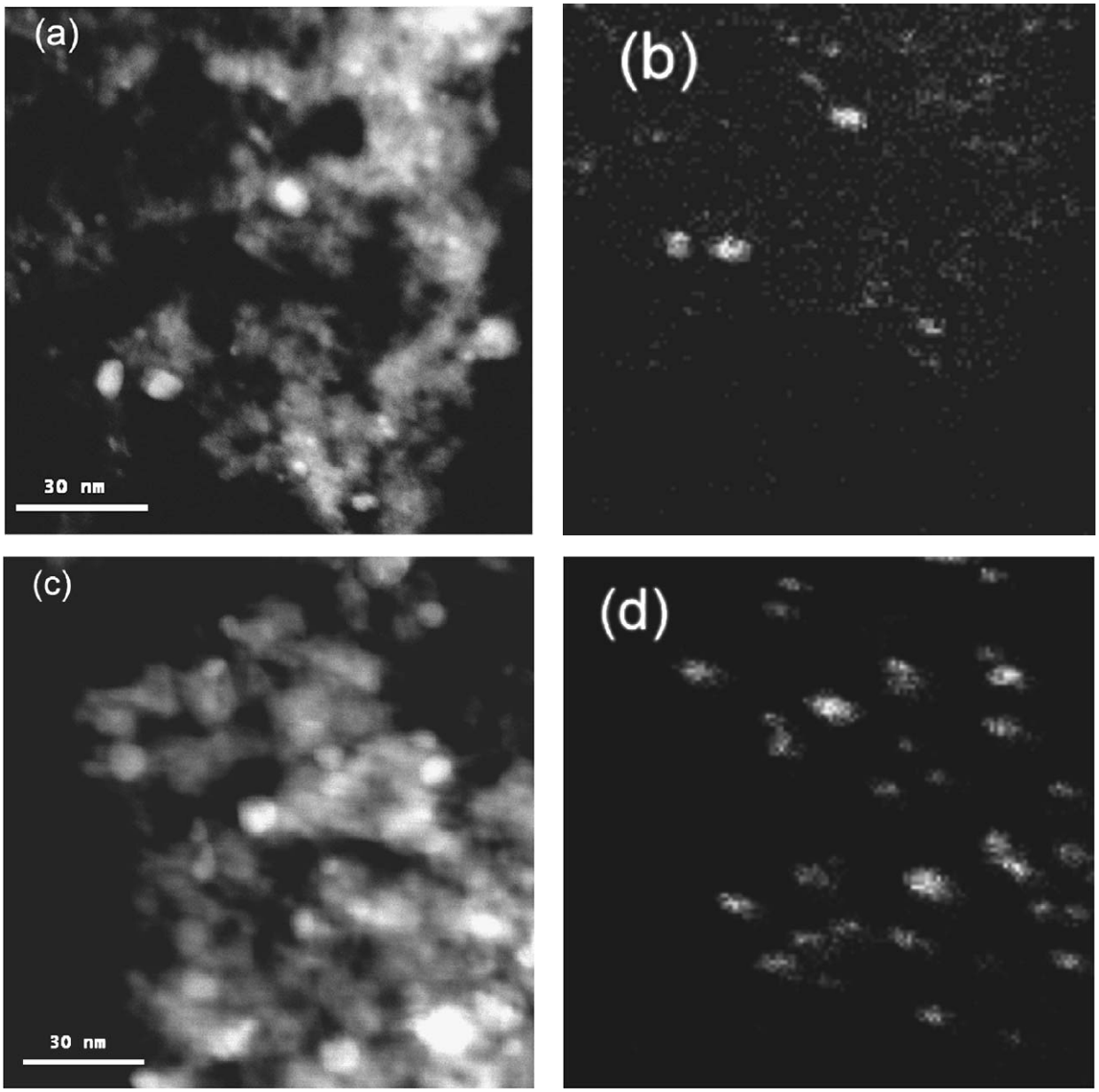

Fig. 3. (a) HAADF image and (b) STEM-XEDS map of the Au M_2 signal for sample A (dried 393 K; high activity); (c, d) HAADF image and STEM-XEDS map for sample B (calcined 673 K; low activity).

samples should have displayed nearly the same activity for CO oxidation. But this was not the case; sample C showed 100% CO conversion at 298 K under our standard test conditions, whereas sample D was inactive even though this sample comprised slightly smaller Au particles. These data clearly demonstrate that gold particle size alone does not control the activity for CO oxidation with these catalysts.

We subsequently prepared more sets of samples by drying batches of the same 5-wt% Au/Fe_2O_3 precursor at 393 K and calcining some of this material at 673 K. By carefully manipulating the drying procedure, we found it is possible to prepare dried samples containing no gold particles rediscernible by our conventional TEM technique (denoted as sample E; Table 1), whereas the corresponding material calcined at 673 K (denoted sample F; Table 1) comprised gold particles with a mean diameter of 3.7 nm (Fig. 7). Significantly, with sample E, a CO conversion of 100% was maintained under standard test conditions for several hours, whereas sample F was inactive under these conditions, even though the mean gold particle size was near optimal for CO oxidation according to recently proposed models for the active site [15].

In view of the lack of discernible gold particles in sample E in our standard TEM experiments, we also characterized samples of this type using HREM; under these conditions, we were able to observe evidence of nanoclusters with diameters $\leqslant$1 nm in the images of some samples (Fig. 8). These nanoclusters were not observed in all of the dried samples that we prepared using this method; often no gold particles were observed at all. The presence of these extremely small nanoclusters, with their large surface area:volume ratios, is consistent with the presence

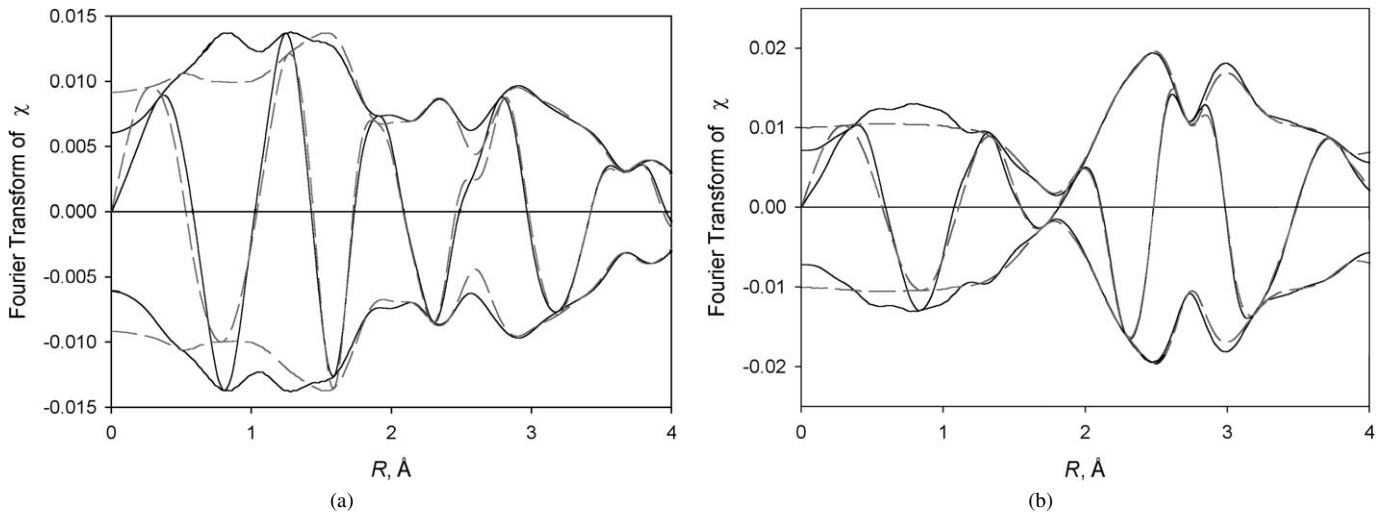

Fig. 4. Results of EXAFS analysis characterizing (a) the dried gold/iron oxide catalyst and (b) the calcined gold/iron oxide catalyst scanned at nearly liquid nitrogen temperature and under vacuum (10^{-5} Torr). Shown are the imaginary part and magnitude of uncorrected Fourier transform (k^0 weighted) of experimental EXAFS function (solid line) and sum of the calculated contributions (dashed line).

Table 2
EXAFS fit parameters characterizing Fe_2O_3-supported gold samples before catalysis[a]

Absorber/ back-scatterer pair	Dried sample				Calcined sample			
	N	R (Å)	$10^3 \times \Delta\sigma^2$ (Å^2)	ΔE_0 (eV)	N	R (Å)	$10^3 \times \Delta\sigma^2$ (Å^2)	ΔE_0 (eV)
Au–Au 1st shell	8.3	2.79	9.12	1.91	10.7	2.85	10.18	1.77
Au–Au 2nd shell	4.1	3.89	8.34	7.27	6.2	3.99	11.12	6.03
Au–O_s	1.4	2.04	1.49	5.51	0.9	2.10	4.13	8.73
Au–O_l	1.3	2.59	0.24	1.02	0.4	2.64	6.31	−2.63

[a] Notation: N, coordination number; R, distance between absorber and backscatterer atoms; $\Delta\sigma^2$, Debye–Waller factor; ΔE_0, inner potential correction. Expected errors: N, ±10%; R, ±0.02 Å; $\Delta\sigma^2$, ±20%; ΔE_0, ±20%. The subscripts s and l refer to short and long, respectively.

of relatively large numbers of interfacial gold atoms that have been suggested to be cationic [36,44]. However, we emphasize that we observed only relatively few of these nanoclusters in these dried samples.

In a further set of experiments, XANES measurements were made during CO oxidation catalysis for samples E and F (Fig. 9). These data showed a striking difference between the dried and calcined samples. The high-activity dried sample E exhibited a sharp peak near 11920 eV, whereas the calcined sample F showed only a weak signal in this vicinity. Furthermore, the higher-energy region of the spectrum characterizing the dried sample E exhibited only broad signals, whereas in the spectrum of the calcined sample (F), much more clearly delineated peaks near 11945 and 11970 eV were seen. This comparison indicates a distinct difference in

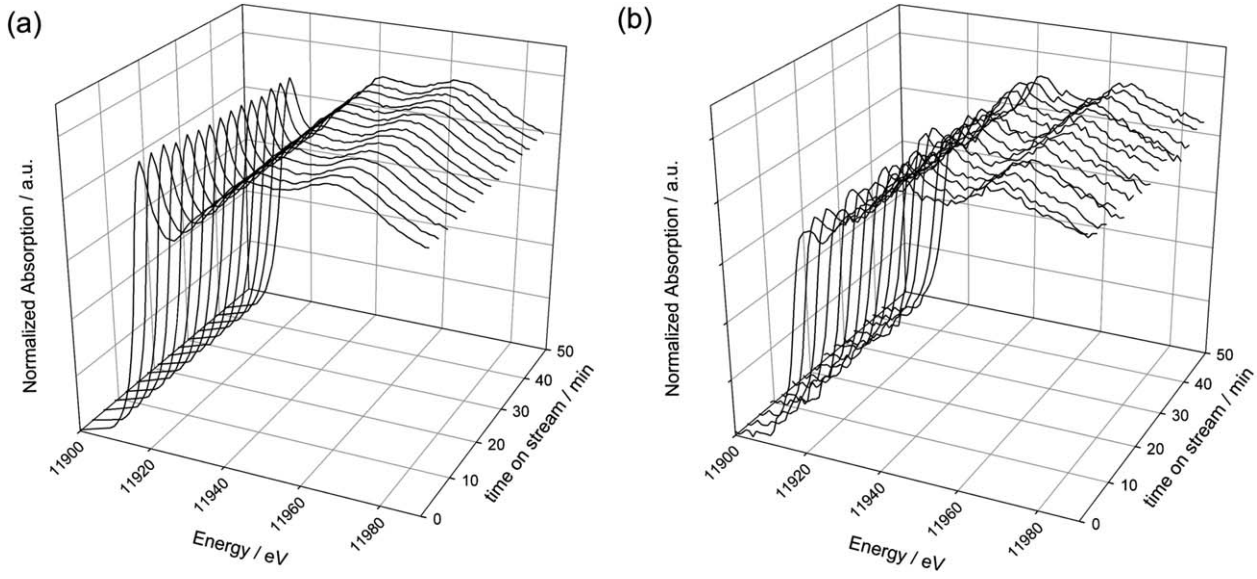

Fig. 5. XANES data characterizing two 5-wt% Au/Fe_2O_3 samples during CO oxidation catalysis. Data are shown for (a) the catalyst dried in flowing air at 393 K (sample A, high activity) and (b) the catalyst calcined at 673 K (sample B, low activity).

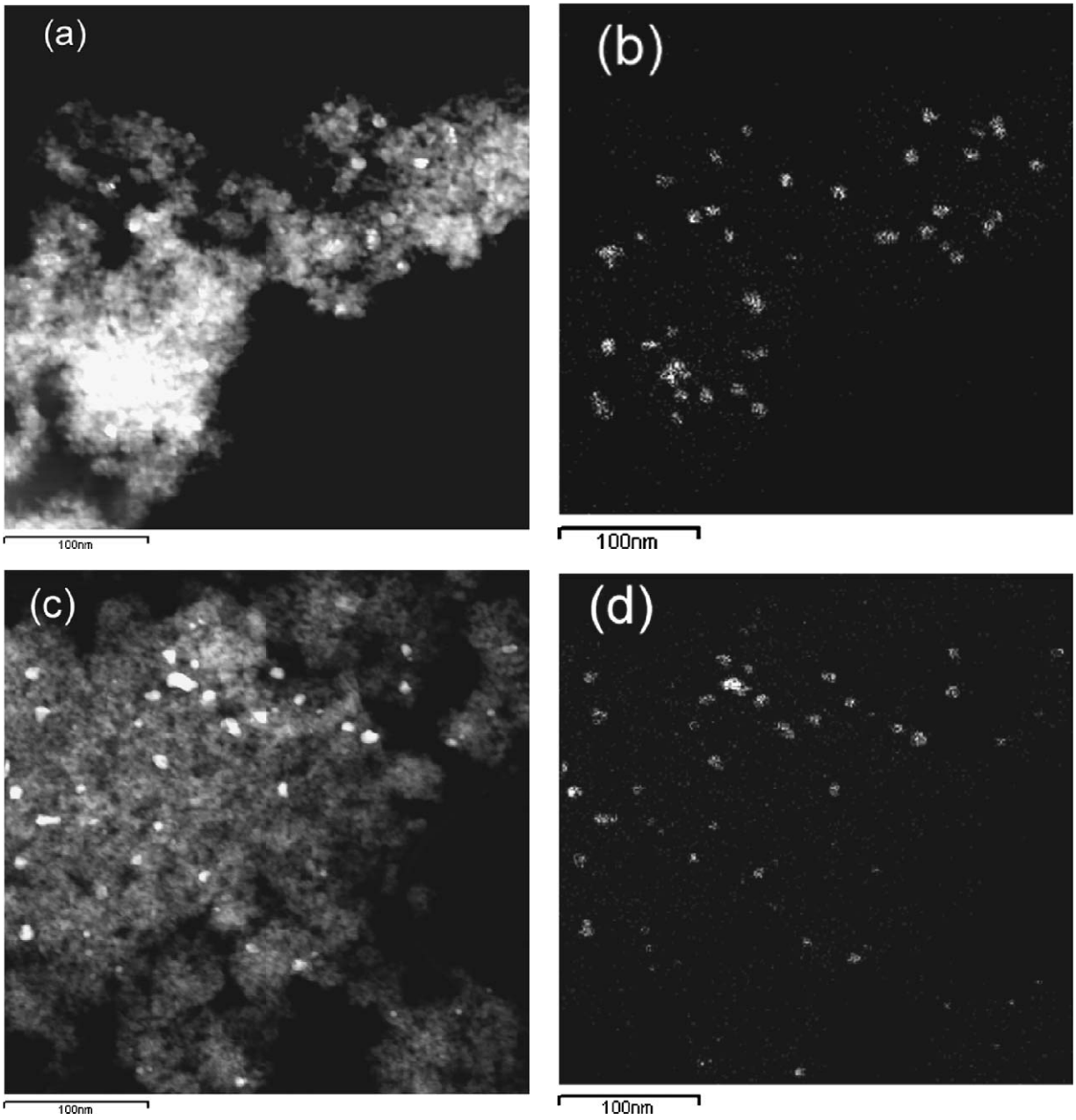

Fig. 6. (a) HAADF image and (b) STEM-XEDS map of the Au M_2 signal for sample C (dried at 393 K in a tube furnace in static air); (c, d) HAADF image and STEM-XEDS map for sample D (dried in a GC oven).

the electronic nature of the gold in the two catalyst samples.

Because the signal near 11,920 eV is typical of cationic gold and the higher-energy signals are typical of metallic gold [35,37], these results indicate that the dried sample E contains primarily cationic gold and the calcined sample F contains primarily metallic gold. As we noted earlier, in situ XANES measurements indicated that the initial oxidation states of the supported gold in each catalyst remained essentially unchanged during CO oxidation catalysis, suggesting that the higher proportion of cationic gold in the uncalcined sample made that catalyst more active than the calcined catalyst, which, as shown by XANES, contained predominantly zerovalent gold.

Because XANES spectra depend on the environment of the gold and not just on its oxidation state, these data do not provide a quantitative basis for estimating how much gold was present in each oxidation state in our samples. Consequently, we turned to one of the most definitive techniques for characterizing and quantifying the relative amounts of cationic gold in highly dispersed samples, ^{197}Au Mössbauer effect spectroscopy [3,20,45,56]. The Mössbauer absorption spectra (Fig. 10; parameters in Table 3) of the high-activity sample E showed that the gold in this catalyst was in the +3 oxidation state. The gold was likely present as Au(III)-oxyhydroxide species, because the spectrum consisted of two doublets characteristic of $AuOOH{\cdot}H_2O$ [20]. The spectra of the less-active

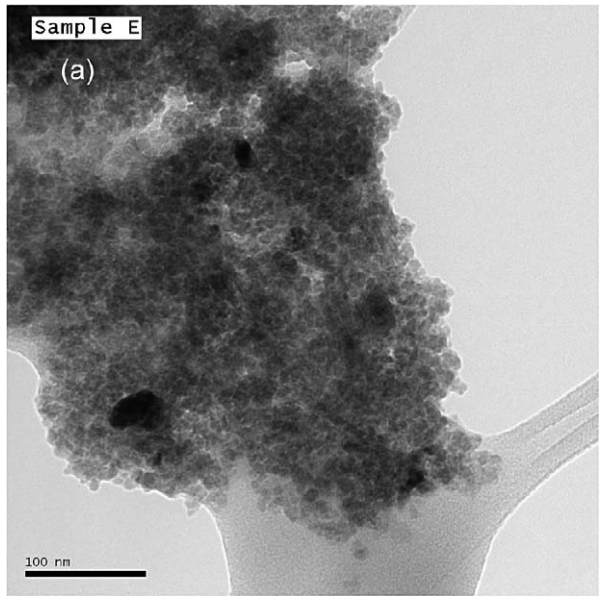

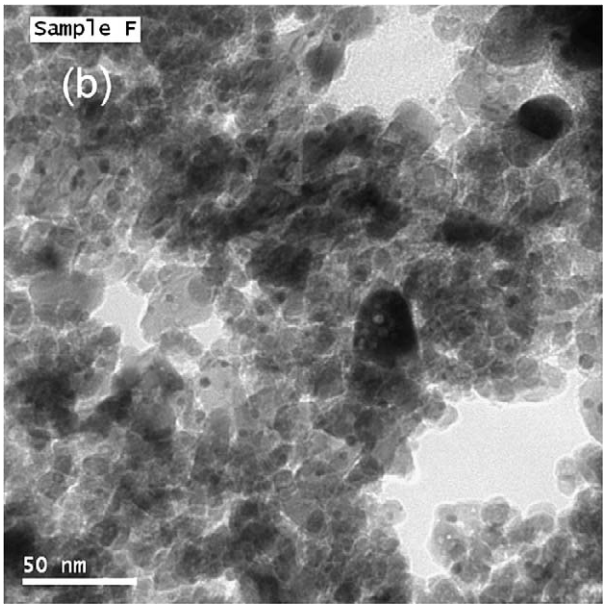

Fig. 7. Bright field TEM micrographs of 5-wt% Au/Fe_2O_3 catalysts: (a) the catalyst dried in flowing air at 393 K (sample E, high activity), and (b) the catalyst calcined at 673 K (sample F, low activity).

calcined sample F exhibited gold in its metallic form. These data indicate that the nanoclusters observed occasionally in the HREM analysis were very much the minority state representing the gold in sample E.

We also measured the Mössbauer spectra of the active sample E after subjecting it to treatment with flowing CO (298 K, 7 h). The data showed no change in the amount of cationic gold in the sample. These results are consistent with the activity data representing this catalyst, which showed a CO conversion of ca. 100% maintained over several hours in the continuous-flow reactor. Our results are fully compatible with the XANES spectra in demonstrating the crucial role of cationic gold in CO oxidation catalysis. Although gold particle size has an effect on the shape of the Mössbauer spectra, this effect is small [56] and

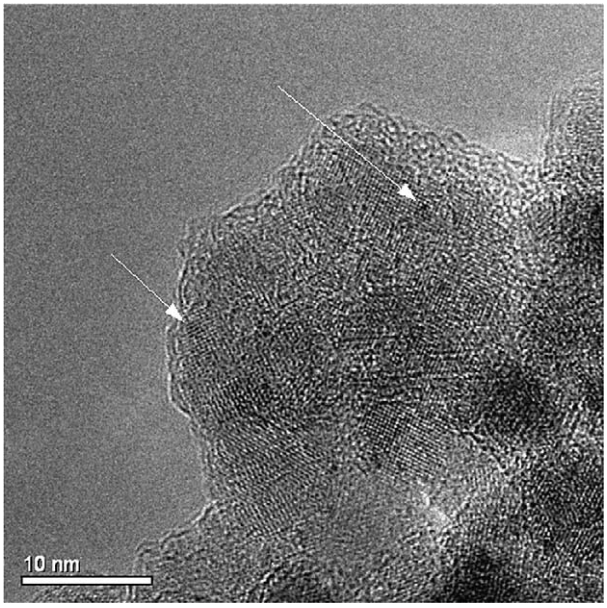

Fig. 8. HREM micrograph of an area of sample E showing occasional subnanometer gold clusters.

cannot explain the significant difference observed between low-activity and high-activity samples.

We also recorded XPS data for samples E and F (Fig. 11). A clear shift to lower binding energy (by 0.9 eV) was observed for the catalyst calcined at 673 K (sample F) relative to that dried at 393 K (sample E). Consistent with the XANES and Mössbauer results, we can assign this shift in binding energy to differences in the nature of the gold species present in the sample, representing the transition from predominantly cationic gold (in the high-activity sample E) to metallic gold (in the low-activity sample F). Thus, we infer that the observed $Au(4f_{7/2})$ binding energy shift (Figs. 2 and 11) arises from differences in the gold cation content of the catalysts. The correlation of catalytic activity for CO oxidation with the oxidation state of gold is consistent with the XANES and Mössbauer spectra characterizing the active and inactive Fe_2O_3-supported catalysts, and it is in qualitative agreement with an earlier report [37] on MgO-supported gold catalysts for CO oxidation. STEM studies of the support for gold catalysts showed a transformation from disordered nanocrystalline iron oxyhydroxide for the catalyst dried at 120 °C to hematite for the calcined sample. XPS analysis of the Fe(2p) spectra showed no significant changes with calcination.

4. Conclusion

In summary, our data—determined with a set of independent, complementary techniques—provide compelling evidence that cationic gold plays a crucial role in CO oxidation catalyzed by Au/Fe_2O_3. The catalyst displaying the highest activity comprises mainly cationic gold, and this persists during operation in a flow reactor under our catalytic reaction conditions. These results, obtained for high-activity supported metal catalysts representative of those used in practical applications, appear to contradict a number of reported interpretations of

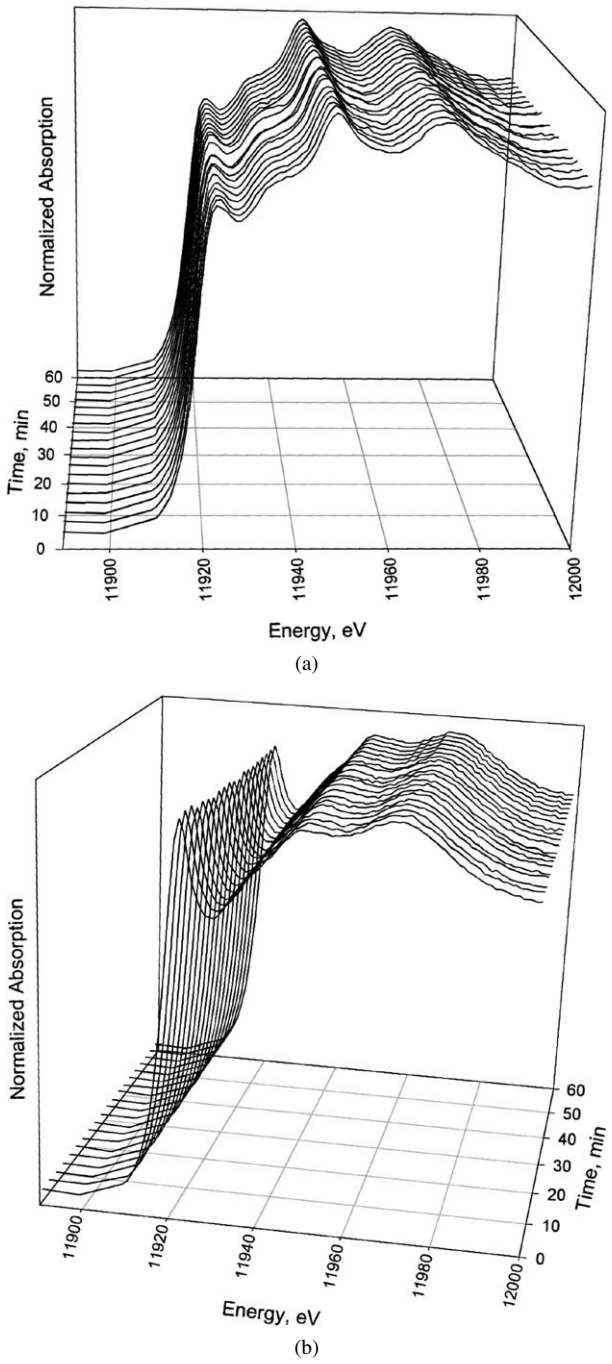

Fig. 9. XANES data characterizing two 5-wt% Au/Fe_2O_3 samples during CO oxidation catalysis. Data are shown for (a) the catalyst dried in flowing air at 393 K (sample E, high activity), and (b) the catalyst calcined at 673 K (sample F, low activity).

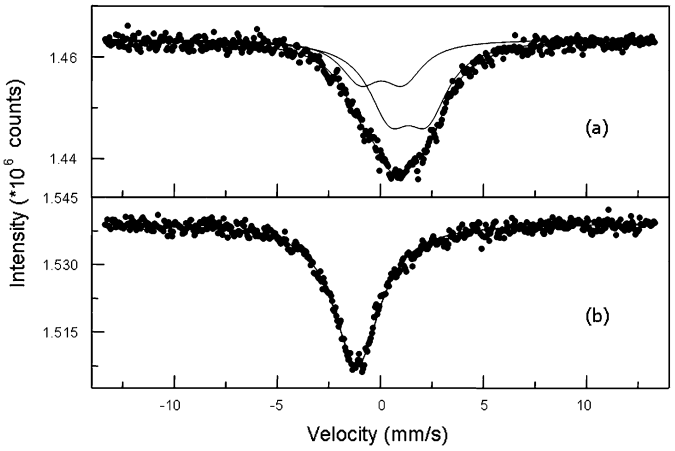

Fig. 10. Mössbauer effect spectra characterizing 5-wt% Au/Fe_2O_3 catalysts for (a) the catalyst dried in flowing air at 393 K (sample E, high activity), and (b) the catalyst calcined at 673 K (sample F, low activity).

Table 3
Mössbauer fit parameters for Fig. 10

Sample	I.S. ($mm\,s^{-1}$)*	Q.S. ($mm\,s^{-1}$)*	L.W. ($mm\,s^{-1}$)*	S.C. (%)*
Au/Fe_2O_3, dried	0.06	2.08	2.31	34.8
	1.37	1.82	2.46	65.2
Au/Fe_2O_3, calcined 400 °C	−1.14	–	2.73	100

* I.S. = isomer shift; Q.S. = quadrupole splitting; L.W. = line width; and S.C. = spectral contribution.

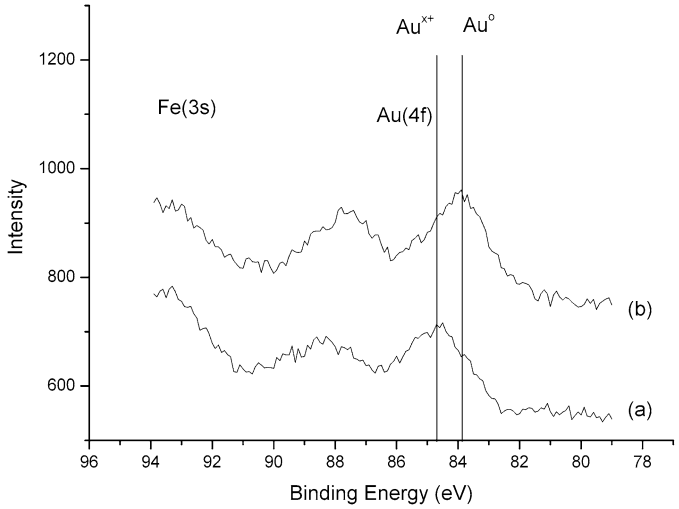

Fig. 11. Au(4f) X-ray photoelectron spectra characterizing 5-wt% Au/Fe_2O_3 catalysts: (a) catalyst dried in flowing air at 393 K (sample E, high activity), and (b) that calcined at 673 K (sample F, low activity).

the nature of the active species in model supported gold catalysts [55]. We recognize that it is possible that our findings are restricted to the system of Fe_2O_3-supported Au catalysts, because these materials appear to be uniquely sensitive to catalyst pretreatment at the drying and calcination stages. However, the reported model studies [55] were carried out with catalysts markedly different from ours, and, in particular, the supports were not hydroxylated.

The previously reported studies of CO oxidation catalyzed by gold on model supports have not used the wide array of available techniques to thoroughly characterize the electronic nature of the gold in the active sites of these catalysts; in particular, techniques capable of determining the presence of cationic gold were not applied. We have shown that these techniques can be incisive in determining the nature of the Au species present in active catalysts, and note that in a recent extensive review [55] concerning the nature of the active gold species in both supported Au nanoparticles and model systems, the use of ^{197}Au Mössbauer effect spectroscopy is not included. In contrast to the

investigations of model systems, we examined catalysts with high activities using a wide range of available techniques, and our data clearly show that gold is present in both metallic and cationic forms in the Au/Fe_2O_3 samples, and that the presence of a significant fraction of cationic gold is essential for high CO oxidation activity. Moreover, our results demonstrate the complexity of a realistic high-area gold catalyst compared with the structurally less-complex model catalysts. Although investigations of such model systems can provide valuable data, they may fall short of permitting a thorough exploration of the subtlety of high-activity supported catalysts of the kind that find technological application. Indeed, in this investigation we have clearly demonstrated the complexity of Au/Fe_2O_3 catalysts; many different structures can be prepared, and only by using a range of spectroscopic and other techniques can this complexity can be unraveled. Our key observation is that the high activity observed by many researchers for CO oxidation at 298 K with Au/Fe_2O_3 catalysts is predicated on the presence of cationic gold that persists under these reaction conditions for extended periods.

Acknowledgments

The authors acknowledge the National Synchrotron Light Source, Brookhaven National Laboratory, which is supported by the US Department of Energy, Division of Materials Sciences and Division of Chemical Sciences, under contract DE-AC02-98CH10886, and the staff of Beamline X-18B. The research at the University of California was supported by the US Department of Energy (grant FG02-04ER15513) and the National Science Foundation (grant CTS-0121619). The research at Cardiff University was supported by the Science and Engineering Research Council and Johnson-Matthey (project ATHENA), the Science and Engineering Research Council (Ph.D. studentship), and the European Union (project AURICAT; contract HPRN-CT-2002-00174). The authors thank the staff at the National Centre for Electron Spectroscopy and Surface Analysis, Daresbury, UK, as well as the generous support of the National Science Foundation Materials Research Science and Engineering Center at Lehigh University (grant NSF DMR-0079996).

References

[1] G.J. Hutchings, J. Catal. 96 (1985) 292.
[2] B. Nkosi, N.J. Coville, G.J. Hutchings, Appl. Catal. 43 (1988) 33.
[3] B. Nkosi, M.D. Adams, N.J. Coville, G.J. Hutchings, J. Catal. 128 (1991) 378.
[4] B. Nkosi, N.J. Coville, G.J. Hutchings, M.D. Adams, J. Friedl, F. Wagner, J. Catal. 128 (1991) 366.
[5] T. Hayashi, K. Tanaka, M. Haruta, J. Catal. 178 (1998) 566.
[6] T.A. Nijhuis, H. Huizinga, M. Makkee, J.A. Moulijn, Ind. Eng. Chem. Res. 38 (1999) 884.
[7] E.E. Stangland, K.B. Stevens, R.P. Andres, W.N. Delgass, J. Catal. 191 (2000) 332.
[8] G. Mul, A. Zwijnenburg, B. Linden, M. van der Makkee, J.A. Moulijn, J. Catal. 201 (2001) 128.
[9] M. Haruta, Catal. Today 36 (1997) 123.
[10] J.E. Bailie, G.J. Hutchings, Chem. Commun. (1999) 2151.
[11] G.C. Bond, D.T. Thompson, Catal. Rev.-Sci. Eng. 41 (1999) 319.
[12] G.C. Bond, D.T. Thompson, Gold Bull. 33 (2000) 41.
[13] M. Haruta, CATTECH 6 (2002) 102.
[14] M. Haruta, M. Date, Appl. Catal. A 222 (2001) 427.
[15] M. Haruta, Gold Bull. 37 (2004) 27.
[16] R. Meyer, C. Lemaire, Sh.K. Shaikutdinov, H.-J. Freund, Gold Bull. 37 (2004) 72.
[17] A.S.K. Hashmi, Gold Bull. 37 (2004) 51.
[18] M. Date, M. Okumura, S. Tsubota, M. Haruta, Angew. Chem. Int. Ed. 43 (2004) 2129.
[19] S. Carrettin, P. Concepcion, A. Corma, J.M. Lopez Nieto, V.F. Puntes, Angew. Chem. Int. Ed. 43 (2004) 2538.
[20] R.M. Finch, N.A. Hodge, G.J. Hutchings, A. Meagher, Q.A. Pankhurst, M.R.H. Siddiqui, F.E. Wagner, R. Whyman, Phys. Chem. Chem. Phys. 1 (1999) 485.
[21] D.T. Thompson, Appl. Catal. A 243 (2003) 201.
[22] G.J. Hutchings, Gold Bull. 29 (1996) 123.
[23] P. Landon, P.J. Collier, A.J. Papworth, C.J. Kiely, G.J. Hutchings, Chem. Commun. (2002) 2058.
[24] P. Landon, P.J. Collier, A.F. Carley, D. Chadwick, A.J. Papworth, A. Burrows, C.J. Kiely, G.J. Hutchings, Phys. Chem. Chem. Phys. 5 (2003) 1917.
[25] J.K. Edwards, B. Solsona, P. Landon, A.F. Carley, A. Herzing, M. Watanabe, C.J. Kiely, G.J. Hutchings, J. Mater. Chem. 15 (2005) 4595.
[26] J.K. Edwards, B.E. Solsona, P. Landon, A.F. Carley, A. Herzing, C.J. Kiely, G.J. Hutchings, J. Catal. 236 (2005) 69.
[27] T. Ishihara, Y. Ohura, S. Yoshida, Y. Hata, H. Nishiguchi, Y. Takita, Appl. Catal. A 291 (2005) 215.
[28] L. Prati, M. Rossi, J. Catal. 176 (1998) 552.
[29] F. Porta, L. Prati, M. Rossi, S. Colluccia, G. Martra, Catal. Today 61 (2000) 165.
[30] C. Bianchi, F. Porta, L. Prati, M. Rossi, Top. Catal. 13 (2000) 231.
[31] L. Prati, Gold Bull. 32 (1999) 96.
[32] S. Carrettin, P. McMorn, P. Johnston, K. Griffin, G.J. Hutchings, Chem. Commun. (2002) 696.
[33] S. Carrettin, P. McMorn, P. Johnston, K. Griffin, C.J. Kiely, G.J. Hutchings, Phys. Chem. Chem. Phys. 5 (2003) 1329.
[34] M.D. Hughes, Y.-J. Xu, P. Jenkins, P. McMorn, P. Landon, A.F. Carley, G.A. Attard, G.J. Hutchings, F. King, E.H. Stitt, P. Johnston, K. Griffin, C.J. Kiely, Nature 437 (2005) 1132.
[35] J.C. Fierro-Gonzalez, B.C. Gates, J. Phys. Chem. B 108 (2004) 16999.
[36] J.C. Fierro-Gonzalez, V.A. Bhirud, B.C. Gates, Chem. Commun. (2005) 5275.
[37] J. Guzman, B.C. Gates, J. Am. Chem. Soc. 126 (2004) 2672.
[38] Q. Fu, H. Saltsburg, M. Flytzani-Stephanopoulos, Science 301 (2003) 935.
[39] M. Valden, X. Lai, D.W. Goodman, Science 281 (1998) 1647.
[40] M.S. Chen, D.W. Goodman, Science 306 (2004) 252.
[41] D.C. Maeir, D.W. Goodman, J. Am. Chem. Soc. 126 (2004) 1892.
[42] V.A. Bondzie, S.C. Parker, C.T. Campbell, Catal. Lett. 63 (1999) 143.
[43] A. Sanchez, S. Abbet, U. Heiz, W.-D. Schneider, H. Häkkinen, R.N. Barnett, U. Landman, J. Phys. Chem. A 103 (1999) 9573.
[44] N. Lopez, J.K. Nørskov, J. Am. Chem. Soc. 124 (2002) 11262.
[45] J. Guzman, S. Carrettin, J.C. Fierro-Gonzalez, Y. Hao, B.C. Gates, A. Corma, Angew. Chem. Int. Ed. 44 (2005) 4778.
[46] N.A. Hodge, C.J. Kiely, R. Whyman, M.R.H. Siddiqui, G.J. Hutchings, Q.A. Pankhurst, F.E. Wagner, R.R. Rajaram, S.E. Golunski, Catal. Today 72 (2002) 133.
[47] R.E. Jentoft, S.E. Deutsch, B.C. Gates, Rev. Sci. Instrum. 67 (1996) 2111.
[48] J.F. Odzak, A.M. Argo, F.S. Lai, B.C. Gates, K. Pandya, L. Feraria, Rev. Sci. Instrum. 72 (2001) 3943.
[49] M. Vaarkamp, J.C. Linders, D.C. Koningsberger, Physica B 209 (1995) 159.
[50] A.F. Carley, M.K. Rajumon, M.W. Roberts, J. Solid State Chem. 106 (1993) 156.
[51] M.G. Mason, Phys. Rev. B 27 (1983) 748.
[52] G.K. Wertheim, S.B. Di Cenzo, S.E. Youngquist, Phys. Rev. Lett. 51 (1983) 2310.

[53] S.B. Di Cenzo, G.K. Wertheim, Comments Solid State Phys. 11 (1985) 203.
[54] C.C. Chusuei, X. Lai, K.I. Luo, D.W. Goodman, Top. Catal. 14 (2001) 71.
[55] M.S. Chen, D.W. Goodman, Catal. Today 111 (2006) 22.
[56] L. Stievano, S. Santucci, L. Lozzi, S. Calogero, F.E. Wagner, J. Non-Cryst. Solids 232–234 (1998) 644.